

Numerical testing of mirror diffusion of cosmic rays

CHAO ZHANG¹ AND SIYAO XU^{a1}

¹*Department of Physics, University of Florida, 2001 Museum Rd., Gainesville, FL 32611, USA*

ABSTRACT

The tension between recent observations and theories on cosmic ray (CR) diffusion necessitates exploration of new CR diffusion mechanisms. We perform the first numerical study on the mirror diffusion of CRs that is recently proposed by Lazarian & Xu (2021). We demonstrate that the perpendicular superdiffusion of turbulent magnetic fields and magnetic mirroring that naturally arise in magnetohydrodynamic (MHD) turbulence are the two essential physical ingredients for the mirror diffusion to happen. In supersonic, subsonic, and incompressible MHD turbulence, with the pitch angles of CRs repeatedly crossing 90° due to the mirror reflection, we find that the mirror diffusion strongly enhances the confinement of CRs, and their pitch-angle-dependent parallel mean free path can be much smaller than the injection scale of turbulence. With the stochastic change of pitch angles due to gyroresonant scattering, CRs stochastically undergo slow mirror diffusion at relatively large pitch angles and fast scattering diffusion at smaller pitch angles, resulting in a Lévy-flight-like propagation.

1. INTRODUCTION

Cosmic ray (CR) diffusion in turbulent and magnetized media is a fundamental problem in space physics and astrophysics. Theoretical studies of CR diffusion have improved our understanding of important astrophysical processes, e.g., planetary and star formation (Rodgers-Lee et al. (2020); Padovani et al. (2020); Semenov et al. (2021)), evolution of galaxies and galaxy clusters (e.g., Guo & Oh (2008); Brunetti & Jones (2014); Holguin et al. (2019); Hopkins et al. (2020); Quataert et al. (2022)). Recently, the new-generation CR observations challenge the existing theoretical paradigm of CR diffusion (e.g., Gabici et al. (2019); Evoli et al. (2020); Amato & Casanova (2021); Fornieri et al. (2021)), which urges us to reexamine the fundamental physics of CR diffusion.

CR diffusion strongly depends on the properties of magnetohydrodynamic (MHD) turbulence that they interact with. Direct simulations of MHD turbulence enable numerical testing of the theoretical models of MHD turbulence (e.g., Maron & Goldreich (2001); Cho & Vishniac (2000); Cho & Lazarian (2002); Cho & Lazarian (2003)) and CR diffusion (e.g., Beresnyak et al. (2011); Xu & Yan (2013); Cohet & Marcowith (2016); Hu et al. (2022); Sampson et al. (2023); Gao & Zhang (2023)). In the presence of magnetic fields, the CR diffusion perpendicular and parallel to the magnetic field needs to be treated separately. Within the inertial range of MHD turbulence, the superdiffusion of turbulent magnetic fields (Lazarian & Vishniac (1999)) causes the perpendicular superdiffusion of CRs (Xu & Yan (2013); Lazarian & Yan (2014); Hu et al. (2022)).

In the direction parallel to the magnetic field, most earlier studies are focused on the diffusion induced by gyrores-

onant scattering. Due to the scale-dependent anisotropy of Alfvén and slow modes in MHD turbulence (Goldreich & Sridhar (1995); Lazarian & Vishniac (1999)), Alfvén and slow modes are inefficient in scattering the CRs with gyro-radii much smaller than the turbulence injection scale (Chandran (2000); Yan & Lazarian (2002); Xu & Lazarian (2020)), while fast modes are identified as the more efficient agent of scattering (Yan & Lazarian (2004)). More recently, strong scattering of CRs by sharp intermittent magnetic field bends in MHD turbulence is proposed to be important for affecting CR parallel diffusion (Lemoine (2023); Kempfski et al. (2023); Butsky et al. (2023)). The enhanced local scattering can be associated with the intermittent and fractal structure of MHD turbulence (Isliker & Vlahos (2003)).

The resonant scattering faces its long-standing 90° problem in the framework of the quasi-linear theory (Jokipii (1966)). To resolve this issue, nonresonant interactions such as magnetic mirroring was explored (Fermi (1949); Cesarsky & Kulsrud (1973), CK73 henceforth; Noerdlinger (1968); Klepach & Ptuskin (1995); Chandran (2000)). This consideration of the mirroring effect naturally solves the 90° problem and limits the pitch angle range for gyroresonant scattering (CK73; Xu & Lazarian (2020)). Magnetic mirrors can naturally form in MHD turbulence due to compressions of magnetic fields, which are induced by pseudo-Alfvénic modes in an incompressible medium and slow and fast modes in a compressible medium. Unlike the trapping effect of magnetic mirrors considered for compressible MHD waves in CK73, Lazarian & Xu (2021) (LX21 henceforth) found that in MHD turbulence due to the perpendicular superdiffusion of turbulent magnetic fields (Lazarian & Yan (2014)), CRs do not experience trapping. Instead, they bounce among different magnetic mirrors and move diffusively along the local magnetic field, which leads to a new diffusion mechanism termed “mirror diffusion”. The mirror diffusion accounts for

Table 1. Parameters of MHD turbulence simulations

MHD Turbulence	M_A	M_s	β	Resolution	L_{inj}	l_{diss}
Compressible subsonic (M1)	0.68	0.60	2.569	792^3	≈ 400	≈ 25
Compressible supersonic (M2)	0.58	10.50	0.006	512^3	≈ 250	≈ 20
Incompressible (M3)	0.80	–	–	512^3	≈ 200	≈ 10

the suppressed diffusion of CRs when the mirroring condition is satisfied (Xu (2021); Barreto-Mota et al. (2023)).

In this work, we will carry out the first numerical test of the mirror diffusion with test particle simulations in MHD turbulence. We will also examine the pitch-angle-dependent mean free path of mirror diffusion that is analytically predicted by LX21. The outline of this letter is as follows. In Section 2, we describe the numerical methods used for the test particle simulations. In Section 3, we present our numerical results on testing the mirror diffusion and measuring its mean free path in different MHD turbulence regimes. Our conclusions can be found in Section 4.

2. NUMERICAL METHODS

For the turbulent magnetic fields used for our test particle simulations, we take snapshots from 3D compressible and incompressible MHD turbulence simulations after the MHD turbulence reaches a statistically steady state. The compressible MHD turbulence simulations are taken from Hu et al. (2022), which are generated via ZEUS-MP/3D code (Hayes et al. (2006)). It solves the ideal MHD equations in a periodic box under the isothermal condition. The turbulence is solenoidally driven in Fourier space with the injected turbulent kinetic energy peaked at wavenumber $k = 2$, which is half of the data cube size, approximately 400 grids for the subsonic data cube (M1 henceforth) and 250 grids for the supersonic data cube (M2 henceforth). The numerical dissipation occurs at $l_{\text{diss}} \approx 20$ grids for M1 with numerical resolution = 792^3 and $l_{\text{diss}} \approx 25$ grids for M2 with numerical resolution = 512^3 . The incompressible MHD turbulence simulation (M3 henceforth) is taken from Cho (2010), which is generated by using the pseudo-spectral code developed by Cho & Vishniac (2000). It solves the incompressible MHD equations in a periodic box with hyperviscosity and hyperdiffusivity. The peak of turbulent energy injection is at $k \approx 2.5$ (corresponding to the turbulence injection scale $L_{\text{inj}} \approx 200$ grids), and the numerical resolution is 512^3 . The numerical dissipation occurs around $l_{\text{diss}} \approx 10$ grids. The inertial range of MHD turbulence is within $[L_{\text{inj}}, l_{\text{diss}}]$. In M1 and M2, the mean magnetic field \vec{B}_0 is in the z direction and in M3 \vec{B}_0 is in the x direction. By applying the hyperviscosity and hyperdiffusivity, M3 has a slightly more extended inertial range compared to M2 with the same resolution. Further details about these simulations can be found in Hu et al. (2022), Cho & Vishniac (2000) and Cho (2010). Since we are interested in the diffusion of relativistic CRs in non-relativistic MHD turbulence, that is, the test particle speed is much greater than the turbulent speed and the Alfvén speed V_A , the turbulent magnetic fields can be treated as a

static background for the test particle and the motional electric field can be neglected¹. The parameters of the three MHD simulations used in this work are summarized in Table 1. MHD turbulence is characterized by the Alfvén Mach number $M_A = V_L/V_A \approx \langle v \rangle / (\langle B \rangle / \sqrt{4\pi\langle \rho \rangle})$, where V_L is the turbulent velocity at L_{inj} , $\langle v \rangle$, $\langle \rho \rangle$ and $\langle B \rangle$ are the rms values of velocities, densities, and magnetic field strength.² The three MHD simulations we use are sub-Alfvénic with $M_A < 1$.³ For compressible MHD turbulence, $M_s = V_L/c_s$ is the sonic Mach number, where c_s is the isothermal sound speed. We include both subsonic ($M_s < 1$) and supersonic ($M_s > 1$) cases for the compressible MHD turbulence.

For our test particle simulations, we inject relativistic test particles that represent CR particles in a snapshot of MHD turbulence simulations. To trace the test particle trajectory, we numerically solve the following equations:

$$\frac{d\vec{u}}{dt} = \frac{q}{\gamma mc} \vec{u} \times \vec{B}, \quad (1)$$

and

$$\frac{d\vec{r}}{dt} = \vec{u}, \quad (2)$$

for a particle of position \vec{r} , velocity \vec{u} , charge q and mass m . \vec{B} is the magnetic field, c is the speed of light, and t is the time. We follow a numerical method similar to that adopted in Xu & Yan (2013); Hu et al. (2022). We use the Bulirsch-Stoer method to integrate Eq. 1 along with 2 with an adaptive time step (Press et al. (1988)). It provides a high accuracy for the particle trajectory integration with a relatively low computational effort (see also López-Barquero et al. (2016)). At each time step, the local magnetic field at the location of a test particle is interpolated by the cubic spline using the magnetic fields of the 10^3 neighbouring points.

The energy of a test particle is well conserved during the simulation and is quantified by the ratio r_L/L_{inj} , where the Larmor radius r_L is defined as

$$r_L = \gamma \frac{mc^2}{qB_0}, \quad (3)$$

¹ We note that the properties of magnetic fields in a snapshot of MHD turbulence simulations are fundamentally different from static magnetic fields. The information on the stochasticity and superdiffusion of turbulent magnetic fields is well preserved in the snapshot.

² Note that M_A is defined as V_L/V_A (Lazarian (2006)). In practice, different methods for measuring M_A in MHD turbulence simulations are introduced (e.g., Xu & Yan (2013); Cohet & Marcowith (2016); Beattie et al. (2022)).

³ In super-Alfvénic turbulence with $M_A > 1$, field line wandering becomes important in affecting the CR diffusion (Brunetti & Jones (2014)). Its comparison with mirror diffusion will be carried out in our future work.

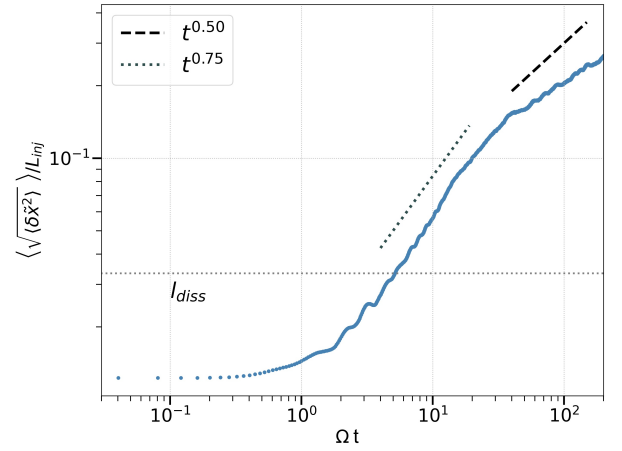
with the Lorentz factor γ . Throughout this paper, we use L_{inj} to normalize length scales as L_{inj} is relatively well determined in our simulations. The gyrofrequency is defined as $\Omega = u/r_L$. At every time step, we measure $\mu = \cos \theta$, where θ is the angle between $\vec{u}(\vec{r})$ and $\vec{B}(\vec{r})$, i.e., the pitch angle of a test particle. To achieve statistically reliable results, we inject a sufficiently large number of test particles and take an ensemble average of the numerical measurements over all test particles.

3. NUMERICAL RESULTS

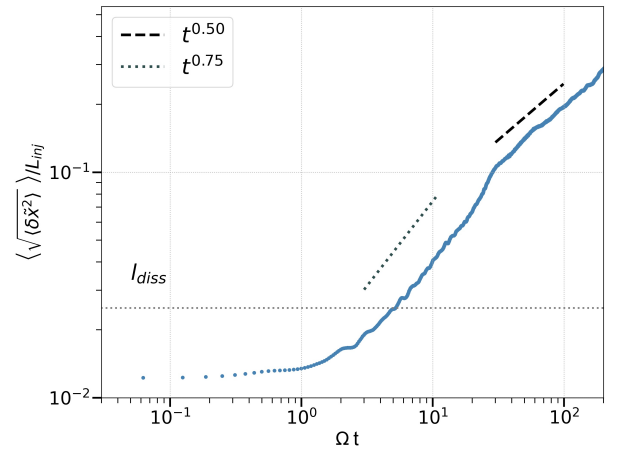
The mirror diffusion of CRs in MHD turbulence arises from both the mirror reflection by magnetic compressions and the perpendicular superdiffusion caused by the Alfvénic turbulence. The latter plays an essential role in enabling the parallel diffusion of mirroring particles (LX21), which would otherwise be trapped between two fixed magnetic mirror points (CK73). To numerically test the mirror diffusion, we will first demonstrate the perpendicular superdiffusion of CRs, which has been analytically studied (Lazarian & Yan (2014); Lazarian et al. (2023)). The previous numerical testing of perpendicular superdiffusion of CRs was performed at small θ (e.g., Xu & Yan (2013); Hu et al. (2022)). To demonstrate the perpendicular superdiffusion of mirroring CRs with large θ (see Section 3.2.1), we will adopt large initial θ .

3.1. Perpendicular Superdiffusion of mirroring CRs

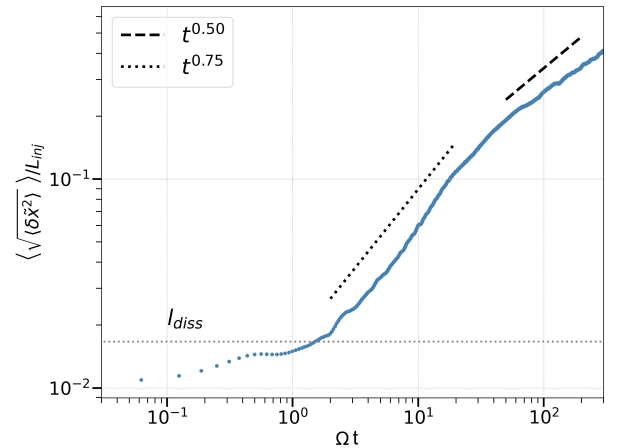
The perpendicular superdiffusion of CRs is caused by that of turbulent magnetic fields and takes place within the inertial range of MHD turbulence (Lazarian & Yan (2014)). To have initially small separations between the particle trajectories, we inject 50 beams of test particles, and each beam consists of 20 particles. Within each beam, the 20 particles are initially randomly distributed within a volume of size of around 5 to 8 grids, so that the average initial separation between a pair of particles is around 3 to 5 grids. All test particles have the same initial pitch angle cosine $\mu_0 \approx 0.10$ and $r_L = 0.01L_{inj}$. Within each beam, we measure the perpendicular separation $\delta\tilde{x}$ of every pair of particle trajectories with respect to \vec{B}_0 and obtain its rms value for all pairs. We then take the average over all beams as the measured perpendicular displacement $\langle \sqrt{\langle \delta\tilde{x}^2 \rangle} \rangle$.



(a) M1



(b) M2



(c) M3

Figure 1. Averaged perpendicular separation of test particles $\langle \sqrt{\langle \delta\tilde{x}^2 \rangle} \rangle$ vs. time for M1 (a), M2 (b) and M3 (c), with $r_L = 0.01L_{inj}$ and initial pitch angle cosine $\mu_0 = 0.10$. l_{diss} is indicated by the horizontal dashed line.

The measured $\langle \sqrt{\langle \delta \tilde{x}^2 \rangle} \rangle$ normalized by L_{inj} for M1, M2 and M3 as a function of t (normalized by Ω^{-1}) is presented in Fig. 1. In all three cases, irrespective of the MHD turbulence regime, perpendicular superdiffusion is observed above l_{diss} (see values in Table 1). Below l_{diss} , CRs undergo subdiffusion with $\sqrt{\langle \delta \tilde{x}^2 \rangle} \propto t^\alpha$ and $\alpha < 0.5$. Above l_{diss} , we see the transition from perpendicular superdiffusion with $\alpha > 0.5$ to perpendicular normal diffusion with $\alpha \approx 0.5$. For the perpendicular superdiffusion, $\alpha = 0.75$ is expected for the case when CRs undergo diffusive motion along the magnetic field (Lazarian et al. (2023)). Our result indicates that the mirroring CRs simultaneously undergo parallel diffusion and perpendicular superdiffusion within the inertial range of MHD turbulence.

3.2. Parallel Mirror Diffusion

3.2.1. Mirror Diffusion

In the presence of a magnetic mirror with a longitudinal magnetic gradient, CRs with r_L smaller than the mirror size l_{\parallel} and μ satisfying

$$\mu < \sqrt{\frac{\delta B_{\parallel}}{B_0 + \delta B_{\parallel}}} \quad (4)$$

can be reflected by the magnetic mirror under the mirror force, where δB_{\parallel} is the parallel magnetic fluctuation over l_{\parallel} and B_0 is the mean magnetic field strength. The mirror force is (CK73)

$$F_{\parallel} = -M \frac{\partial B_{\parallel}}{\partial l_{\parallel}}, \quad (5)$$

where M is the magnetic moment

$$M = \frac{\gamma m u_{\perp}^2}{2B}, \quad (6)$$

where u_{\perp} is the perpendicular component of \vec{u} . For mirroring CRs with their motion along the magnetic field dominated by magnetic mirroring, there is no stochastic change of μ , and M is a constant, known as the first adiabatic invariant. As an example, in Fig. 2 we present the trajectory of one test particle with $r_L = 0.01L_{\text{inj}}$ and $\mu_0 = 0.05$ in M2. We adopt a sufficiently small r_L ($< L_{\text{diss}}$) for mirroring to dominate over gyroresonant scattering and a sufficiently small μ_0 for the condition in Eq. (4) to be satisfied. The smallest r_L is limited by our numerical resolution. In fact, $r_L = 0.01L_{\text{inj}}$ is close to the smallest numerically resolvable scale, i.e., the grid size. In Fig. 2 (a), the particle trajectory is color coded by B/B_0 , where B is the magnetic field strength. The corresponding F_{\parallel} points toward a region with a weaker B/B_0 . It can be seen that the particle is reflected at different mirror points (i.e., regions with stronger B) multiple times and move back and forth in the direction parallel to the magnetic field. However, in the direction perpendicular to the \vec{B}_0 in the z direction, the particle is not trapped due to the perpendicular superdiffusion of turbulent magnetic fields (see Section

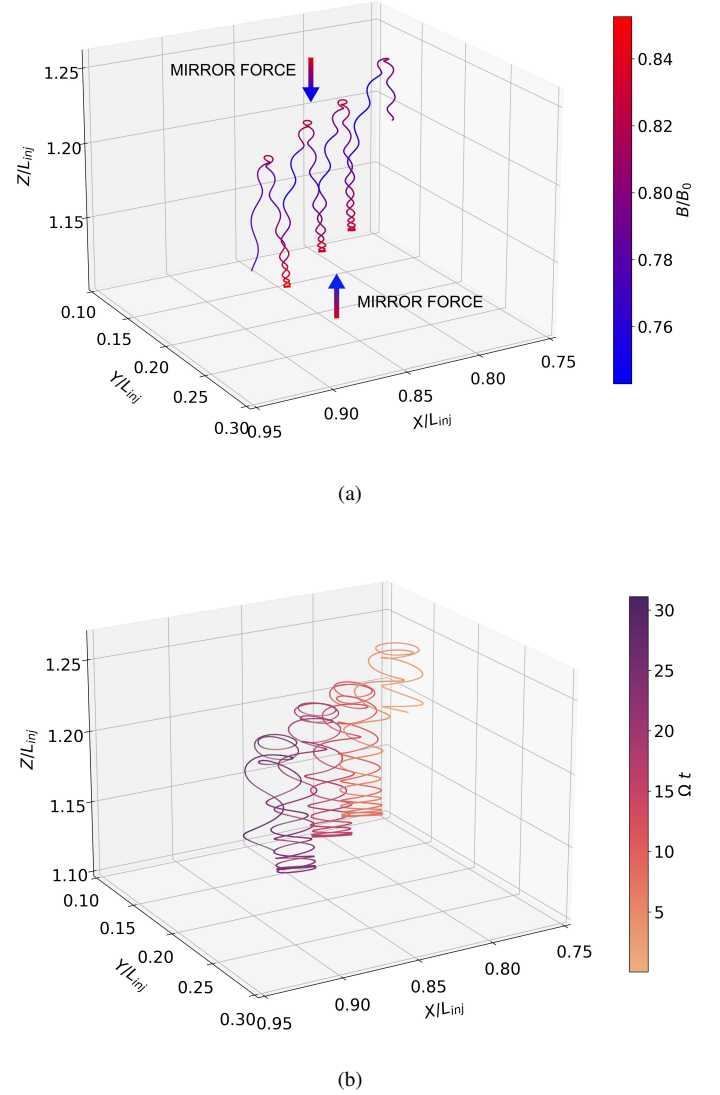


Figure 2. Trajectory of a test particle in M2 with $r_L = 0.01L_{\text{inj}}$ and $\mu_0 = 0.05$. The trajectory is color coded by magnetic field strength in (a) and time in (b). Trajectories in (a) and (b) are the same except that the trajectory in (a) is averaged over the gyro-period Ω^{-1} to better illustrate the motion of the test particle. Arrows in (a) indicate the directions of mirror forces.

3.1). As expected, CRs are not trapped between two magnetic mirror points, but diffusively move along the magnetic field in MHD turbulence due to the perpendicular superdiffusion.

3.2.2. Transition between mirror diffusion and scattering diffusion

CRs with sufficiently small μ (see Eq. 4) are subject to the nonresonant mirroring interaction and undergo the mirror diffusion. For CRs with larger μ , their parallel diffusion is dominated by the resonant pitch-angle scattering and undergo the scattering diffusion (LX21). The transition between mirror diffusion and scattering diffusion takes place as

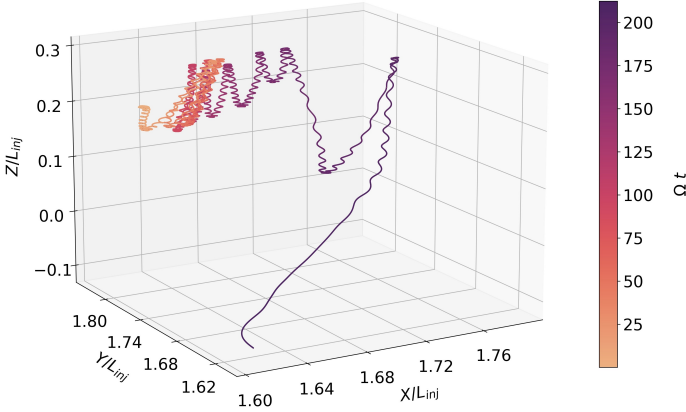


Figure 3. Gyro-averaged trajectory of a test particle in M2 with $r_L = 0.02L_{inj}$ and $\mu_0 = 0.05$. The trajectory is color coded by time, with a transition from mirror diffusion to scattering diffusion.

μ stochastically changes due to the gyroresonant scattering. According to LX21, the transition between the two diffusion regimes is expected to occur at a critical μ as μ_c . In compressible MHD turbulence, under the consideration that fast modes are mainly responsible for mirroring and scattering, μ_c is given by (LX21)

$$\mu_c = \min\{\mu_{\max}, \mu_{\text{eq}}\}, \quad (7)$$

where

$$\mu_{\max} = \sqrt{\frac{\delta B_f}{B_0 + \delta B_f}}, \quad (8)$$

and

$$\mu_{\text{eq}} \approx \left[\frac{14}{\pi} \left(\frac{\delta B_f}{B_0} \right)^2 \left(\frac{r_L}{L_{inj}} \right)^{\frac{1}{2}} \right]^{\frac{2}{11}} \quad (9)$$

corresponds to the pitch angle cosine where mirroring and scattering are in balance, with δB_f as the magnetic fluctuation at L_{inj} of fast modes. Via mode decomposition (see Cho & Lazarian (2003); Lazarian & Pogosyan (2012)), we find that $\delta B_f/B_0$ is close to 0.40 for both M1 and M2, yielding $\mu_{\max} \approx 0.52$. For incompressible MHD turbulence, pseudo-Alfvén modes are responsible for mirroring. Under the consideration of inefficient scattering by Alfvén and pseudo-Alfvén modes for CRs with $r_L \ll L_{inj}$, we have (LX21)

$$\mu_{\max} = \sqrt{\frac{\delta B_s}{B_0 + \delta B_s}}, \quad (10)$$

where δB_s is the magnetic fluctuation of pseudo-Alfvén modes at L_{inj} . As pseudo-Alfvén modes are slaved to Alfvén modes (Beresnyak & Lazarian (2019)), $\delta B_s/B_0$ can be approximately by M_A . Therefore, we have $\mu_c \approx \sqrt{M_A/(1+M_A)}$ for M3. At $\mu < \mu_c$, mirroring dominates

scattering, and CRs are expected to undergo the mirror diffusion. At $\mu > \mu_c$, scattering becomes dominant, and CRs are expected to undergo the scattering diffusion.

Next we numerically demonstrate the transition between the two different diffusion regimes. Here we choose a slightly larger r_L compared to that in Fig. 2 for particles to undergo more scattering. As shown in Fig. 3, from the trajectory of a test particle with $r_L = 0.02L_{inj}$ and $\mu_0 = 0.05$ in M2, we can clearly see the transition from the slow mirror diffusion within a small region to the fast scattering diffusion over a large distance. During the mirror diffusion, the particle is confined in the direction of \vec{B}_0 (the z direction) with multiple mirror reflections. While during the scattering diffusion, the particle does not reverse its moving direction and rapidly moves along the magnetic field.

Furthermore, in Fig. 4 we present the time evolution of μ , particle position in the z direction, and $2M/mu^2$ corresponding to the particle trajectory shown in Fig. 3. The numerical measurements and their gyro-averaged results are shown by blue and orange lines, respectively. Before $\Omega t \approx 200$, we see oscillations of μ around $\mu = 0$, i.e., $\theta = 90^\circ$, which corresponds to the mirror reflection at the mirror points. Accordingly, the particle moves back and forth in the z direction (middle panel in Fig. 4). After $\Omega t \approx 200$, μ changes stochastically, and the particle is not confined in the z direction. The transition between mirror diffusion and scattering diffusion occurs at $\mu \approx 0.5$, which is consistent with our estimate for μ_{\max} in M2 (see Eq. 8). As expected, M is conserved during the mirror diffusion, but varies dramatically during the scattering diffusion as efficient scattering violates the first adiabatic invariant (lower panel in Fig. 4). The distinctive features of mirror diffusion and scattering diffusion can also be seen in simulations with a lower resolution (see Appendix).

The transition between mirror diffusion and scattering diffusion happens due to the stochastic change of μ caused by scattering. To illustrate the stochastic change of μ , in Fig. 5, we present the time evolution of the probability density distribution of μ of 5000 particles with $r_L = 0.01L_{inj}$ and $\mu_0 = 0.05$ in M2. We see that due to the stochastic scattering, the distribution of μ gradually evolves into a more uniform distribution. As a result, CRs stochastically undergo the slow mirror diffusion when $\mu < \mu_c$ and the fast scattering diffusion when $\mu > \mu_c$, leading to a Lévy-flight-like propagation.

3.2.3. Pitch-angle-dependent Parallel Mean Free Path of Mirror Diffusion

For the scattering diffusion, the scattering mean free path corresponds to the change of μ over the range $[\mu_c, 1]$ (CK73; LX21). In the presence of the mirror diffusion at $\mu < \mu_c$, the 90° problem of scattering, i.e., the vanishing scattering near 90° (Jokipii (1966)), is naturally solved, and the scattering mean free path becomes finite. For the mirror diffusion, its parallel mean free path λ_{\parallel} is determined by the size of the magnetic mirrors that the mirroring particles mainly interact with (LX21). For CRs with $\mu < \mu_c$, they preferentially

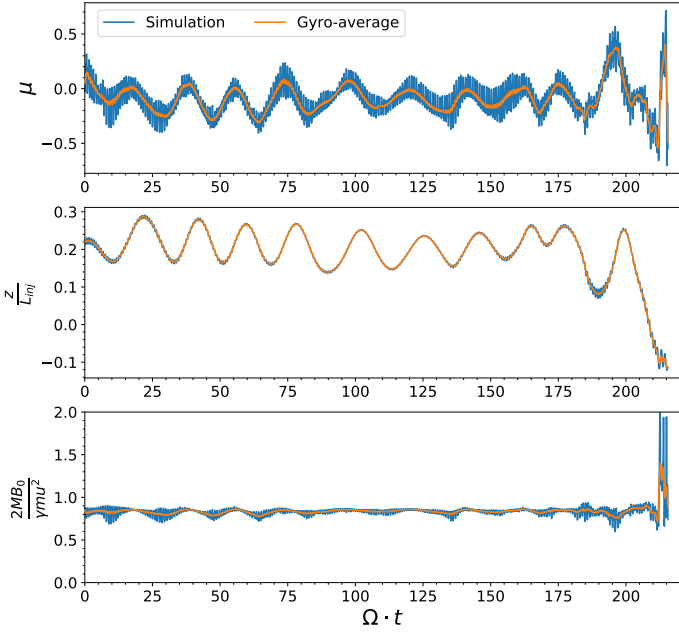


Figure 4. Time evolution of μ , particle position in z direction (the direction of the mean magnetic field for M2) z/L_{inj} , and $2MB_0/\gamma mu^2$ corresponding to the test particle trajectory in Fig. 3. Blue and orange lines represent the numerical measurements and their gyro-averaged results, respectively.

interact with the mirrors satisfying (CK73; Xu & Lazarian (2020))

$$\mu = \sqrt{\frac{\delta b(l_{\parallel})}{B_0 + \delta b(l_{\parallel})}}, \quad (11)$$

where l_{\parallel} is the mirror size, and $\delta b(l_{\parallel})$ is the parallel magnetic fluctuation at l_{\parallel} . Along the energy cascade of MHD turbulence, toward smaller scales, $\delta b(l_{\parallel})$ decreases, but the magnetic field gradient $\delta b(l_{\parallel})/l_{\parallel}$ increases, and the corresponding mirroring becomes more efficient (see Eq. 5). The above equation suggests that among the mirrors with sufficiently large magnetic fluctuations to reflect the CRs with μ , the smallest ones dominant the mirroring. Therefore, λ_{\parallel} of mirror diffusion is expected to depend on μ (LX21). λ_{\parallel} quantifies the slow diffusion of CR particles with sufficiently large pitch angles in the vicinity of CR sources (e.g., Xu (2021)).

To test the μ -dependence of λ_{\parallel} , we inject test particles with different μ_0 . For the particles that exhibit oscillations within the same range $[-\mu, \mu]$, we measure their displacement Δz in the z direction between two mirror points (see Fig. 4 as an illustration) and take the average as the measured mean free path parallel to \vec{B}_0 corresponding to μ . For sub-Alfvénic turbulence, magnetic field lines are mildly perturbed by turbulence especially at small scales. Our measurement serves

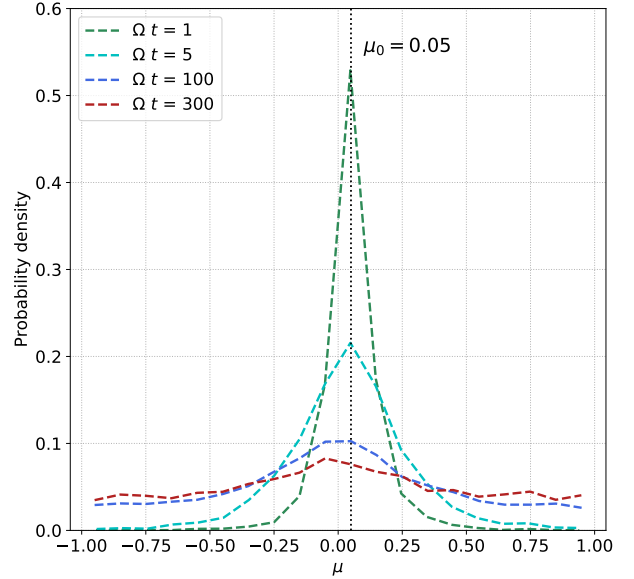


Figure 5. Distributions of μ measured at different times for 5000 test particles with $r_L = 0.01L_{inj}$ and $\mu_0 = 0.05$ (indicated by the vertical dotted line) in M2. The bin size of μ is 0.05.

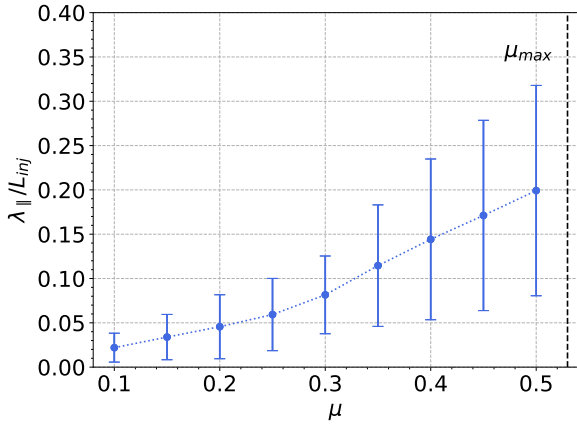
as a good approximation of λ_{\parallel} parallel to the local magnetic field at small μ .

In Fig. 6, we present the measured λ_{\parallel} as a function of μ for M1, M2, and M3 up to the theoretically estimated μ_{max} (Eqs. (8) and (10)). The width of each μ bin is 0.05, and the number of test particles in each μ bin ranges from 50 to 100. We adopt $r_L = 0.01L_{inj} \lesssim l_{diss}$ (see Table 1) for all the test particles to suppress the gyroresonant scattering, but the nonresonant mirroring is still active. Therefore, we have $\mu_c \approx \mu_{max}$ for both compressible and incompressible MHD turbulence. In all three MHD turbulence regimes, we see that λ_{\parallel} increases with increasing μ within the range $\mu < \mu_{max}$, as predicted by LX21. The error bar represents the standard deviation σ and also increases with increasing μ . At a given μ , we find that Δz has a distribution (see Fig. 7). As the degree of field line wandering increases toward larger scales, the deviation of the local magnetic field direction from the mean magnetic field direction becomes more significant at large scales. This may give rise to a larger σ of the Δz distribution at a larger μ (see Fig. 7).

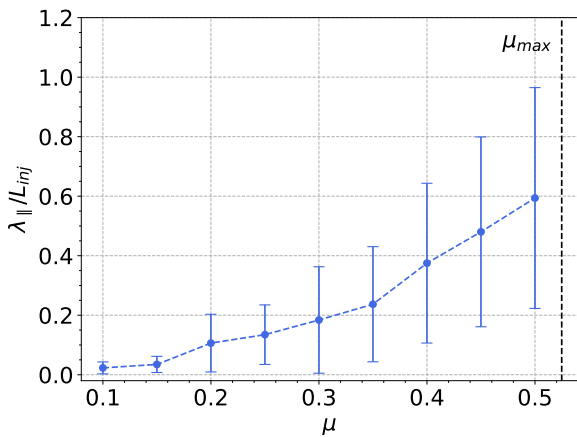
4. CONCLUSIONS

With test particle simulations in MHD turbulence, we performed the first numerical test of mirror diffusion of CRs. Here we summarize our main findings.

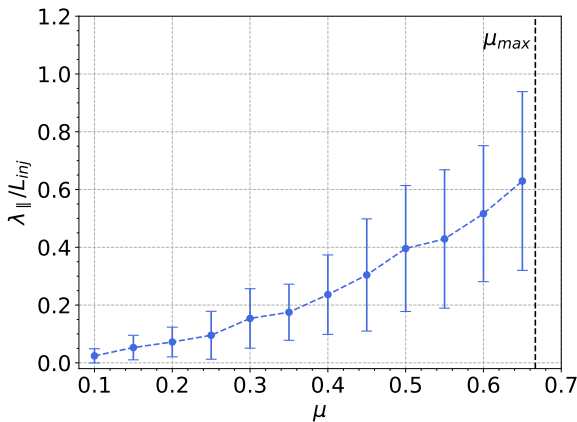
(1) We identify the CRs with $\mu < \mu_c$ as mirroring CRs, which are subject to the mirror reflection by magnetic compressions in both compressible and incompressible MHD turbulence. We find that the mirroring CRs simultaneously un-



(a) M1



(b) M2



(c) M3

Figure 6. Parallel mean free path $\lambda_{\parallel}/L_{inj}$ for mirror diffusion measured at different μ for M1, M2, and M3. The vertical dashed lines indicate the estimated μ_{max} , which is ≈ 0.52 (Eq. (8)) for M1 and M2 and ≈ 0.67 (Eq. (10)) for M3.

dergo the superdiffusion perpendicular to the mean magnetic

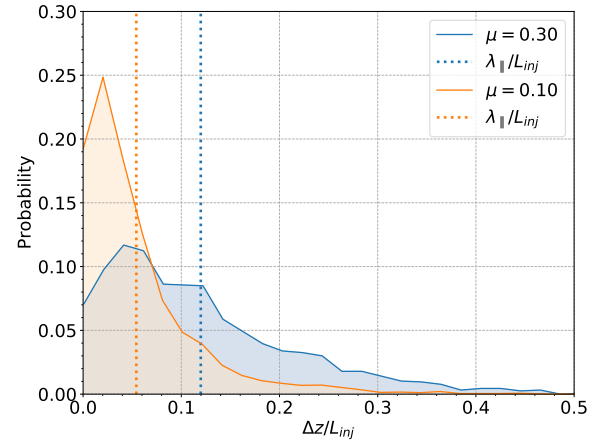


Figure 7. Distribution of parallel displacement Δz measured for test particles with $r_L = 0.01L_{inj}$ and different values of μ in M1. The bin size of Δz is about $0.05L_{inj}$. The vertical dotted lines indicate the mean values.

field and mirror diffusion along the turbulent magnetic field. Rather than being trapped between two fixed magnetic mirror points, the perpendicular superdiffusion enables encounters of mirroring CRs with different magnetic mirrors and their diffusion parallel to the magnetic field.

(2) We numerically demonstrated the distinctive features of mirror diffusion and scattering diffusion. The diffusion of mirroring CRs is characterized by the oscillations in μ around $\mu = 0$. As mirroring CRs repeatedly reverse their moving direction along the magnetic field, the mirror diffusion strongly enhances the confinement of CRs. By contrast, the scattering diffusion violates the first adiabatic invariant and is characterized by the stochastic change of μ within the range $[\mu_c, 1]$. As scattering CRs do not reverse their moving direction, they are weakly confined and rapidly diffuse along the magnetic field. The transition between the two diffusion regimes occurs due to the pitch-angle scattering.

(3) We numerically measured the parallel mean free path of mirror diffusion, which can be much smaller than the turbulence injection scale and increases with increasing μ .

Our numerical measurements are in general consistent with the analytical predictions by LX21. As a new diffusion mechanism of CRs, the mirror diffusion has important implications. Around CR sources, e.g., supernova remnants (Xu (2021)), pulsar wind nebulae, the mirror diffusion of CRs with sufficiently large pitch angles can account for their slow diffusion, as indicated by gamma-ray observations (e.g., Abeysekera et al. (2017); Evoli et al. (2018)). In addition, the mirror diffusion of pickup ions is important for interpreting the Interstellar Boundary Explorer (*IBEX*) ribbon (Xu & Li (2023)). In the Galactic diffuse medium away from CR sources, CRs stochastically undergo slow mirror diffusion and fast scattering diffusion. This Lévy-flight-like propagation of CRs that we find is different from existing models of

CR diffusion solely based on pitch-angle scattering. Its confrontation with CR observations will be further investigated.

ACKNOWLEDGMENTS

We thank Yue Hu for helpful discussions. S.X. acknowledges the support for this work provided by NASA through the NASA Hubble Fellowship grant # HST-HF2-51473.001-A awarded by the Space Telescope Science Institute, which is operated by the Association of Universities for Research in Astronomy, Incorporated, under NASA contract NAS5-26555. This work used SDSC Expanse CPU in SDSC through the allocation PHY230032 from the Advanced Cyberinfrastructure Coordination Ecosystem: Services & Support (ACCESS) program, which is supported by National Science Foundation grants #2138259, #2138286, #2138307, #2137603, and #2138296.

REFERENCES

- Abeysekara, A., Albert, A., Alfaro, R., et al. 2017, *The Astrophysical Journal*, 843, 40
- Amato, E., & Casanova, S. 2021, *Journal of Plasma Physics*, 87, 845870101
- Barreto-Mota, L., de Gouveia Dal Pino, E. M., Lazarian, A., & Xu, S. 2023, in prep.
- Beattie, J. R., Krumholz, M. R., Skalidis, R., et al. 2022, *Monthly Notices of the Royal Astronomical Society*, 515, 5267
- Beresnyak, A., & Lazarian, A. 2019, *Turbulence in magnetohydrodynamics*, Vol. 12 (Walter de Gruyter GmbH & Co KG)
- Beresnyak, A., Yan, H., & Lazarian, A. 2011, *The Astrophysical Journal*, 728, 60
- Brunetti, G., & Jones, T. W. 2014, *International Journal of Modern Physics D*, 23, 1430007
- Butsky, I. S., Nakum, S., Ponnada, S. B., et al. 2023, *Monthly Notices of the Royal Astronomical Society*, 521, 2477
- Cesarsky, C. J., & Kulsrud, R. M. 1973, *The Astrophysical Journal*, 185, 153
- Chandran, B. D. 2000, *The Astrophysical Journal*, 529, 513
- Cho, J. 2010, *The Astrophysical Journal*, 725, 1786
- Cho, J., & Lazarian, A. 2002, *Physical Review Letters*, 88, 245001
- . 2003, *Monthly Notices of the Royal Astronomical Society*, 345, 325
- Cho, J., & Vishniac, E. T. 2000, *The Astrophysical Journal*, 539, 273
- Cohet, R., & Marcowith, A. 2016, *Astronomy & Astrophysics*, 588, A73
- Evoli, C., Gaggero, D., Vittino, A., et al. 2018, *Journal of Cosmology and Astroparticle Physics*, 2018, 006
- Evoli, C., Morlino, G., Blasi, P., & Aloisio, R. 2020, *Physical Review D*, 101, 023013
- Fermi, E. 1949, *Physical review*, 75, 1169
- Fornieri, O., Gaggero, D., Cerri, S. S., De La Torre Luque, P., & Gabici, S. 2021, *Monthly Notices of the Royal Astronomical Society*, 502, 5821
- Gabici, S., Evoli, C., Gaggero, D., et al. 2019, *International Journal of Modern Physics D*, 28, 1930022
- Gao, N., & Zhang, J. 2023, arXiv preprint arXiv:2311.09554
- Goldreich, P., & Sridhar, S. 1995, *Astrophysical Journal, Part 1 (ISSN 0004-637X)*, vol. 438, no. 2, p. 763-775, 438, 763
- Guo, F., & Oh, S. P. 2008, *Monthly Notices of the Royal Astronomical Society*, 384, 251
- Hayes, J. C., Norman, M. L., Fiedler, R. A., et al. 2006, *The Astrophysical Journal Supplement Series*, 165, 188
- Holguin, F., Ruszkowski, M., Lazarian, A., Farber, R., & Yang, H. K. 2019, *Monthly Notices of the Royal Astronomical Society*, 490, 1271
- Hopkins, P. F., Chan, T., Garrison-Kimmel, S., et al. 2020, *Monthly Notices of the Royal Astronomical Society*, 492, 3465
- Hu, Y., Lazarian, A., & Xu, S. 2022, *Monthly Notices of the Royal Astronomical Society*, 512, 2111
- Islaker, H., & Vlahos, L. 2003, *Physical review E*, 67, 026413
- Jokipii, J. R. 1966, *Astrophysical Journal*, vol. 146, p. 480, 146, 480
- Kempski, P., Fielding, D. B., Quataert, E., et al. 2023, arXiv preprint arXiv:2304.12335
- Klepach, E., & Ptuskin, V. 1995, *Astronomy Letters, Volume 21, Issue 3, May 1995*, pp. 411-417; *Pis' ma v Astronomicheskii Zhurnal*, Vol. 21, p. 462, 21, 411
- Lazarian, A. 2006, *The Astrophysical Journal*, 645, L25

- Lazarian, A., & Pogosyan, D. 2012, *The Astrophysical Journal*, 747, 5
- Lazarian, A., & Vishniac, E. T. 1999, *The Astrophysical Journal*, 517, 700
- Lazarian, A., & Xu, S. 2021, *The Astrophysical Journal*, 923, 53
- Lazarian, A., Xu, S., & Hu, Y. 2023, *Frontiers in Astronomy and Space Sciences*, 10, 1154760
- Lazarian, A., & Yan, H. 2014, *The Astrophysical Journal*, 784, 38
- Lemoine, M. 2023, arXiv preprint arXiv:2304.03023
- López-Barquero, V., Farber, R., Xu, S., Desiati, P., & Lazarian, A. 2016, *The Astrophysical Journal*, 830, 19
- Maron, J., & Goldreich, P. 2001, *The Astrophysical Journal*, 554, 1175
- Noerdlinger, P. D. 1968, *Physical Review Letters*, 20, 1513
- Padovani, M., Ivlev, A. V., Galli, D., et al. 2020, *Space Science Reviews*, 216, 29
- Press, W. H., Vetterling, W. T., Teukolsky, S. A., & Flannery, B. P. 1988, *Numerical recipes* (Citeseer)
- Quataert, E., Thompson, T. A., & Jiang, Y.-F. 2022, *Monthly Notices of the Royal Astronomical Society*, 510, 1184
- Rodgers-Lee, D., Vidotto, A., Taylor, A., Rimmer, P., & Downes, T. 2020, *Monthly Notices of the Royal Astronomical Society*, 499, 2124
- Sampson, M. L., Beattie, J. R., Krumholz, M. R., et al. 2023, *Monthly Notices of the Royal Astronomical Society*, 519, 1503
- Semenov, V. A., Kravtsov, A. V., & Caprioli, D. 2021, *The Astrophysical Journal*, 910, 126
- Xu, & Li. 2023, submitted to *ApJ*
- Xu, S. 2021, *The Astrophysical Journal*, 922, 264
- Xu, S., & Lazarian, A. 2020, *The Astrophysical Journal*, 894, 63
- Xu, S., & Yan, H. 2013, *The Astrophysical Journal*, 779, 140
- Yan, H., & Lazarian, A. 2002, *Physical review letters*, 89, 281102
- . 2004, *The Astrophysical Journal*, 614, 757

APPENDIX

A. MIRROR DIFFUSION IN A LOW-RESOLUTION MHD SIMULATION

Unlike the resonant scattering, for the nonresonant mirroring interaction, the corresponding mirror diffusion of CRs at a given μ does not depend on r_L as long as the length scale of magnetic fluctuations is larger than r_L . In this work, we focus on the mirror diffusion of CRs with $r_L \lesssim l_{\text{diss}}$, for which the resonant scattering is suppressed. This provides us a “clean” test of mirror diffusion. For CRs with $r_L > l_{\text{diss}}$, the transition μ_c between mirror diffusion and scattering diffusion depends on r_L , and thus the overall diffusion also depends on r_L (Lazarian & Xu (2021)). We will study the CR propagation with r_L within the inertial range of turbulence in our future work.

Here we examine whether the mirror diffusion of CRs with $r_L \lesssim l_{\text{diss}}$ can also be studied with a lower-resolution MHD simulation. We note that in a lower-resolution simulations, it becomes more challenging to both fully resolve r_L and have r_L much less than l_{diss} given the more limited dissipation range and inertial range. Under these considerations, we adopt a slightly greater $r_L = 0.04L_{\text{inj}}$ ($\lesssim l_{\text{diss}}$) for the test particle simulation in M4 of resolution 256^3 , which is obtained by smoothing M2 by averaging 8 nearest neighboring grids. The parameters of M4 are listed in Table 2, which are similar to those of M2. To compare with the results obtained from M2, we measure the time evolution of μ , z , and M of test particles in M4 and show one example in Fig. 8. Similar to Fig. 4, this particle experiences mirroring with oscillations in μ and z and constant M , but in this example, we see that the transition from mirroring to scattering appears earlier, probably because the scattering is less suppressed as r_L is closer to l_{diss} .

Table 2. Parameters of MHD turbulence simulation with a low resolution

MHD Turbulence	M_A	M_s	β	Resolution	L_{inj}	l_{diss}
Compressible supersonic (M4)	0.41	10.44	0.003	256^3	≈ 120	≈ 8

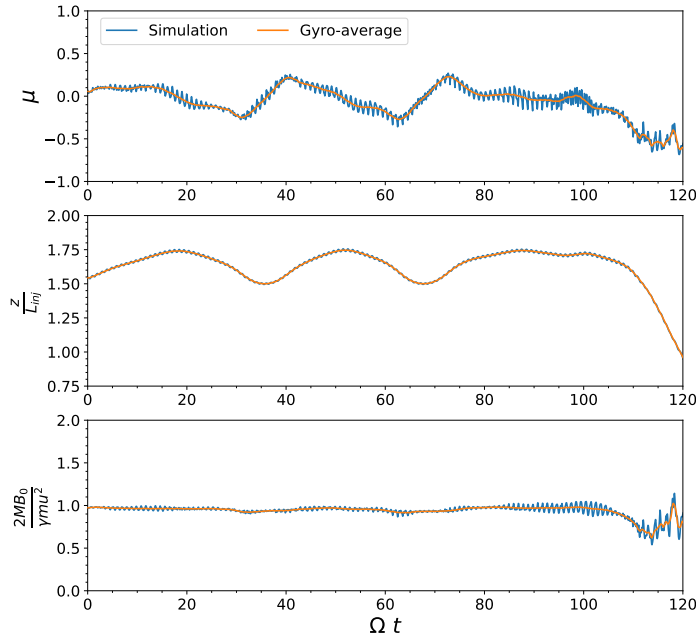


Figure 8. Time evolution of μ , position in z direction z/L_{inj} , and $2MB_0/\gamma mu^2$ for a test particle with $r_L = 0.04L_{\text{inj}}$ and $\mu_0 \approx 0.05$ in M4. Blue and orange lines represent the numerical measurements and their gyro-averaged results, respectively.